Integration of rock anisotropy in the GEMTIP model

Jean-Luc Gagnon & Charles L. Bérubé

Polytechnique Montréal

Introduction

Effective medium theory (**EMT**) is a fundamental approach for modelling complex arrangements of various materials (Pan, 2019; Zhang and Wu, 2015). In the context of induced polarization (**IP**), EMT is used to relate the physical parameters of inclusions within a host rock to the rock's measured effective electrical conductivity.

The Generalized Effective Medium Theory of Induced Polarization (**GEMTIP**, Zhdanov, 2008) model enhances the Cole-Cole model by incorporating physical properties of rock media. This poster aims to further refine the GEMTIP model by integrating anisotropic Green's functions and triaxial ellipsoidal inclusions. These enhancements impact the depolarization tensors, which are computed, compared, and analyzed in the following sections.

Green's function formulation

The complex conductivity tensor is

$$\boldsymbol{\sigma}(\mathbf{r}) = \Delta\boldsymbol{\sigma}(\mathbf{r}) + \boldsymbol{\sigma}_b, \tag{1}$$

where $\boldsymbol{\sigma}_b = \mathrm{diag}(\sigma_{b,x}, \sigma_{b,y}, \sigma_{b,z})$ is the volume average of the background conductivity and $\Delta\boldsymbol{\sigma}(\mathbf{r})$ is the conductivity perturbation caused by the inclusions. The next step involves the quasi-static Maxwell equations with

$$\nabla \cdot \left(\nabla \times \mathbf{B} + \epsilon_0\mu_0 \frac{\partial \mathbf{E}}{\partial t}\right) = \mu_0 \nabla \cdot \mathbf{J} \implies \nabla \cdot \mathbf{J} = 0. \tag{2}$$

Ohm's law, $\mathbf{J} = \boldsymbol{\sigma}\mathbf{E}$, is then used inside the inclusion where no accumulation of charge occurs, yielding

$$\nabla \cdot -\boldsymbol{\sigma}_b \mathbf{E}(\mathbf{r}) = \nabla \cdot (\boldsymbol{\Delta\sigma}(\mathbf{r})\mathbf{E}(\mathbf{r})). \tag{3}$$

Equation 3 then facilitates a Green's function formulation that incorporates the boundary surface field of the IP effect (Zhdanov, 2008), which we write as

$$\mathbf{E}(\mathbf{r}) = \mathbf{E}_0 + \mathbf{E}_0\boldsymbol{\xi}\boldsymbol{\chi}\underbrace{\int_S \nabla\nabla' G(\mathbf{r},\mathbf{r}')\hat{\mathbf{n}}(\mathbf{r}')\hat{\mathbf{n}}(\mathbf{r}')\,\mathrm{d}S}_{\boldsymbol{\Lambda}} + \mathbf{E}_0\boldsymbol{\chi}\underbrace{\int_V \nabla\nabla' G(\mathbf{r},\mathbf{r}')(\mathbf{r}')\,\mathrm{d}V}_{\boldsymbol{\Gamma}}, \tag{4}$$

where $\boldsymbol{\Gamma}$ and $\boldsymbol{\Lambda}$ are the volume and surface depolarization tensors, respectively. $\boldsymbol{\chi}(\mathbf{r}) \cdot \mathbf{E_0} = \Delta\boldsymbol{\sigma}(\mathbf{r})\mathbf{E_0}$ is the material property tensor, $\boldsymbol{\xi}(\mathbf{r}) = \kappa\left(\Delta\boldsymbol{\sigma}(\mathbf{r})\right)^{-1}\boldsymbol{\sigma}_b\boldsymbol{\sigma}(\mathbf{r})$ is the relative material property tensor and $\mathbf{E_0}$ is the applied field (Zhdanov, 2008). Simplifications $\boldsymbol{\xi}(\mathbf{r}) \approx \boldsymbol{\xi}$ and $\boldsymbol{\chi}(\mathbf{r}) \approx \boldsymbol{\chi}$ are valid under the quasi linear approximation. The depolarizing effect of $\boldsymbol{\Gamma}$ and $\boldsymbol{\Lambda}$ are shown in Figure 1.

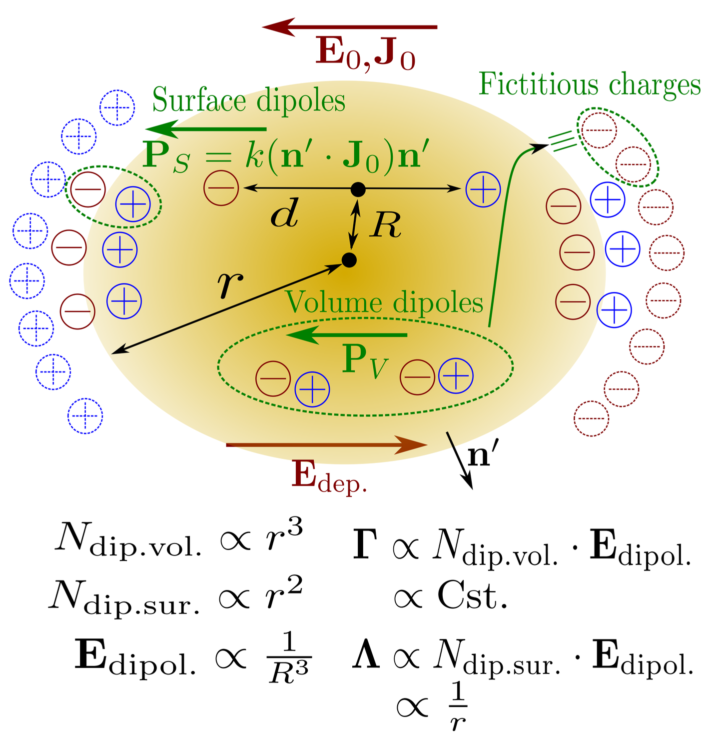

Figure 1. Schematic of an inclusion in a host media and behaviour of $\boldsymbol{\Gamma}, \boldsymbol{\Lambda}$ as functions of inclusion size (Kittel, 2004; Zhdanov, 2008).

The tensors integrals in Equation 4 are then developed using the **anisotropic Green's function** $G(\mathbf{R}, \mathbf{R}')$, after Stroud (1975) and Apresyan and Vlasov (2014), reading

$$G(\mathbf{R}, \mathbf{R}') = \frac{1}{4\pi\sigma_s\,|\mathbf{R} - \mathbf{R}'|}, \tag{5}$$

where the variable change $(\mathbf{R}, \mathbf{R}') = (\mathbf{r}, \mathbf{r}')/\boldsymbol{\sigma}_b^{1/2}$ is used to relate the expression to the spherical coordinates in

$$\mathbf{r}' = a\sin(\theta)\cos(\phi)\,\hat{\mathbf{x}} + b\sin(\theta)\sin(\phi)\,\hat{\mathbf{y}} + c\cos(\theta)\,\hat{\mathbf{z}}$$

and

$$\mathbf{n}' = a^{-1}\sin(\theta)\cos(\phi)\,\hat{\mathbf{x}} + b^{-1}\sin(\theta)\sin(\phi)\,\hat{\mathbf{y}} + c^{-1}\cos(\theta)\,\hat{\mathbf{z}},$$

where a, b and c are the ellipsoidal semi-axes lengths along the x, y, and z axes, respectively, and θ and ϕ are the inclination and azimuth angles, respectively.

Anisotropic ellipsoidal properties

Following the derivation steps in Bérubé and Gagnon (2024), the volume depolarization tensor is

$$\boldsymbol{\Gamma} = -\frac{abc}{4\pi\sigma_s}\mathbf{T}\int_0^{2\pi}\int_0^{\pi}\frac{\mathrm{d}\theta\mathrm{d}\phi\,|\sin\theta|}{|\mathbf{R}'|^3}\mathbf{n}'\mathbf{R}', \tag{6}$$

with $\mathbf{T} = \boldsymbol{\sigma}_b^{-1/2}$, and the surface depolarization tensor is

$$\boldsymbol{\Lambda} = -\frac{abc}{4\pi\sigma_s}\int_0^{2\pi}\int_0^{\pi}\frac{\mathrm{d}\theta\mathrm{d}\phi\,\sin\theta}{|\mathbf{R}'|^5|\mathbf{n}'|}\mathbf{Q}', \tag{7}$$

with $\mathbf{Q}' = \left(-3(\mathbf{R}'\mathbf{R}') + |\mathbf{R}'|^2\mathbf{I}\right)\mathbf{n}'\mathbf{n}'\mathbf{T}^2$, $\sigma_s = \det(\boldsymbol{\sigma}_b)^{1/2}$.

It is important to note that the volume depolarization tensor is now integrated over the surface, using a corollary of the divergence theorem. This approach is analogous to transforming volume dipoles into fictitious surface charges (see Figure 1). According to Milton (2002), the analytical solution for volume depolarization can be expressed using elliptic functions of the first kind (F) and the second kind (E) provided that $a' = a/\sqrt{\sigma_{b,x}} > b' = b/\sqrt{\sigma_{b,y}} > c' = c/\sqrt{\sigma_{c,z}}$. Also, for spheres ($a = b = c$) in isotropic media ($\sigma_{b,x} = \sigma_{b,y} = \sigma_{b,z}$) one finds

$$\boldsymbol{\Gamma} = \frac{1}{3\boldsymbol{\sigma}_\mathbf{b}}, \quad \boldsymbol{\Lambda} = \frac{2}{3a\boldsymbol{\sigma}_\mathbf{b}}, \tag{8}$$

which is consistent with Zhdanov (2008).

Methodology

a) The calculated depolarization tensor $\hat{\boldsymbol{\Gamma}}, \hat{\boldsymbol{\Lambda}}$ of randomly chosen anisotropy parameters $A = b/a$, $B = c/a$ and $C = \sigma_{b,y}/\sigma_{b,x}$, $D = \sigma_{b,z}/\sigma_{b,x}$ are validated using the significant digit metric

$$p = -\log_{10}\left\|\frac{\hat{\boldsymbol{\Gamma}}, \hat{\boldsymbol{\Lambda}} - \boldsymbol{\Gamma}, \boldsymbol{\Lambda}}{\boldsymbol{\Gamma}, \boldsymbol{\Lambda}}\right\| \tag{9}$$

used with the Frobenius matrix norm. For the surface depolarization tensors, a confirmation using work on revolution ellipsoids inclusions in isotropic bulk media from Zhdanov et al. (2018) is done. The p values are averaged ($\overline{p}$) over an interval of variable size with every values of A, B, C, D picked within this interval of mean $\overline{\Pi}$ to increase clarity. The Python *torchquad* (TQ) library and its Simpson's rule integration (SRI) implementation is used to integrate with a fixed number of sample points $N_{\mathrm{spl.}}$.

b) The non-uniform Metropolis-Hasting (MH) sampling method is used to improve the integrand evaluations, since the functions are quite discontinuous. Then, a trapezoidal scheme is used to perform the integration over a triangulated unstructured mesh.

c) The $\boldsymbol{\Gamma}, \boldsymbol{\Lambda}$ are calculated and compared to their simplified solutions $\boldsymbol{\Gamma}', \boldsymbol{\Lambda}'$ for a revolution ellipsoid ($b = c$) and a simple model that modifies the conductivity in the given direction to adjust for the anisotropy in the depolarization tensor (see Equation 8).

Results

a) Figure 2 shows that are our depolarization tensor estimations are in agreement with the literature, having up to six exact/consistent digits when using $N_{\mathrm{spl.}} = 10^4$. For the volume depolarization tensors, the $\overline{p}$ values decrease with increasing anisotropy.

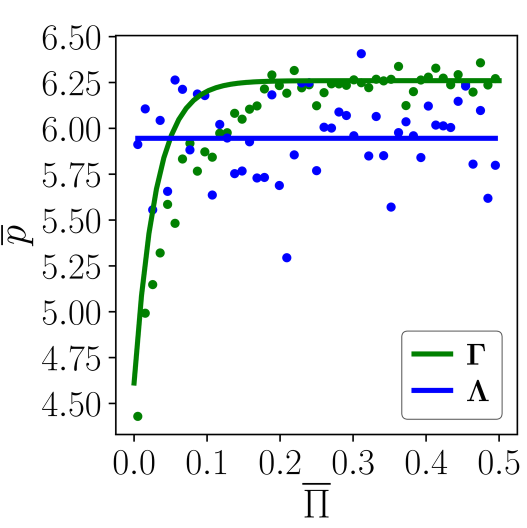

Figure 2. Number of exact/consistent digits on $\boldsymbol{\Gamma}, \boldsymbol{\Lambda}$.

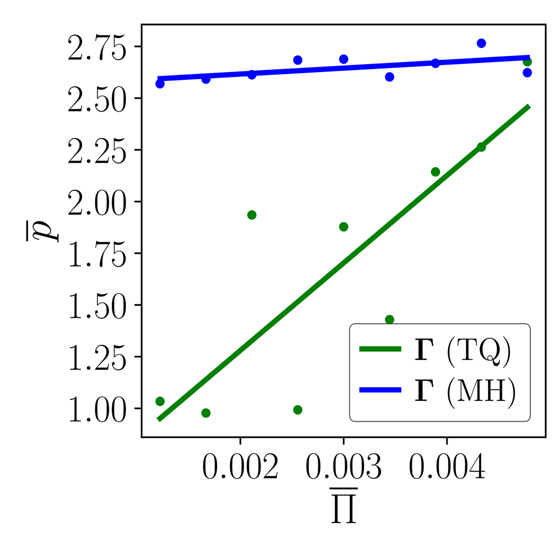

Figure 3. $\overline{p}$ value of $\boldsymbol{\Gamma}$ with TQ and MH at high anisotropy.

b) Figure 3 shows that using the MH algorithm improves the $\overline{p}$ value from 1.5 to 2.5 at high anisotropy. However, the runtime of MH is ≈ 50 times longer than TQ.

Results (continued)

c) Figure 4 shows that the scale dependence of all the surface depolarization tensor elements is consistent with Equation 8 for $a \geq 2$ mm. The longer axis has the lowest depolarization tensor, showing consistence with the volume depolarization tensor in Figure 6. Along with the previous remark, the reduction in $\Lambda_{x,y,z}$ at $a \leq 2\,\mathrm{mm}$ could be explained by the surface dipoles at the edges of the inclusion (see Figure 1), cancelling $\mathbf{E}_{\mathrm{dep.}}$ in the inclusion center, thus reducing $\Lambda_{x,y,z}$. This interpretation is also corroborated by Figure 7 which shows a decrease in the sum of $\boldsymbol{\Lambda}$ as the inclusion size is decrease, while the sum of $\boldsymbol{\Gamma}$ stays constant, in agreement with Kittel (2004).

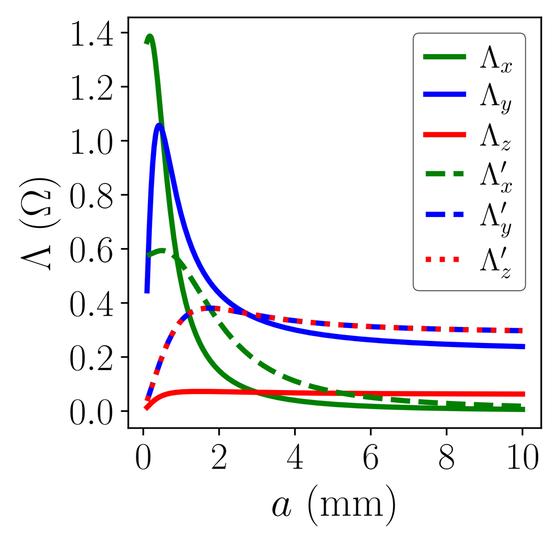

Figure 4. Tensors as a function of a. For $\boldsymbol{\Gamma}$, $(b, c) = (0.5, 3)$ mm and for $\boldsymbol{\Gamma}'$, $b = c = 1.75$ mm. For both models, $\boldsymbol{\sigma}_b = \boldsymbol{I}$.

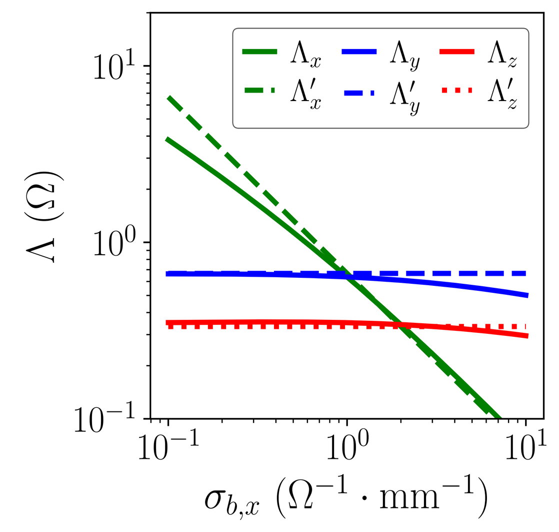

Figure 5. Tensors as a function of $\sigma_{b,x}$. For both models, $(\sigma_{b,y}, \sigma_{b,z}) = (1, 2)\ \Omega^{-1}$·mm^{-1} and $a = b = c = 1$ mm.

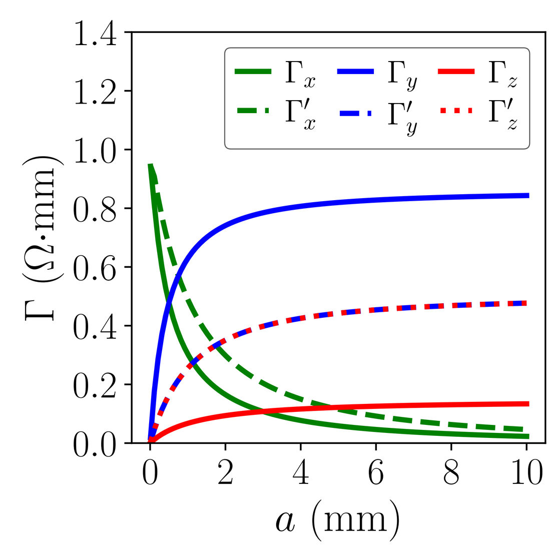

Figure 6. Tensors as a function of a. For $\boldsymbol{\Gamma}$, $(b, c) = (0.5, 3)$ mm and for $\boldsymbol{\Gamma}'$, $b = c = 1.75$ mm. For both models, $\boldsymbol{\sigma}_b = \boldsymbol{I}$.

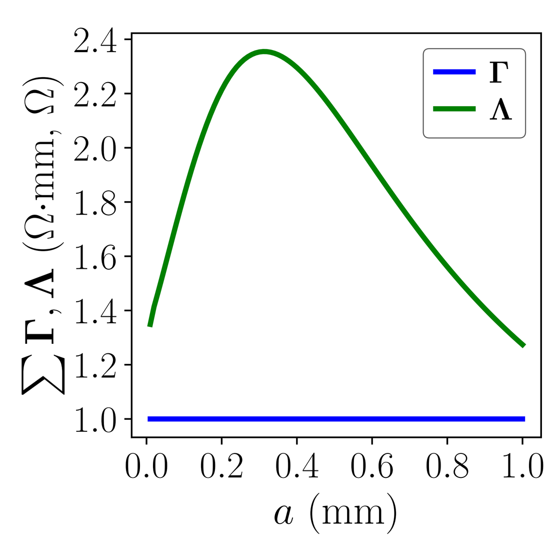

Figure 7. Tensors sum as a function of a. For $\boldsymbol{\Gamma}$, $(b, c) = (0.5, 3)$ mm and for $\boldsymbol{\Gamma}'$, $b = c = 1.75$ mm. Again, $\boldsymbol{\sigma}_b = \boldsymbol{I}$.

Errors on $\boldsymbol{\Gamma}, \boldsymbol{\Lambda}$ range from 10% to 50% using simplified ellipsoids. The impact of $\sigma_{b,x}$ is smaller but still noticeable at reasonable bulk anisotropy $C, D \approx 2, 3$. Thereby, considering a, b, c and $\sigma_{b,x}, \sigma_{b,y}, \sigma_{b,z}$ is important to predict the depolarization tensors in any direction.

Clear differences exist between the simplified and anisotropic GEMTIP models. IP researchers may find the latter useful for modelling the effective conductivity of anisotropic rocks and soils or strengthening interpretations of IP data collected in multiple directions.

Conclusions

An anisotropic Green's function was incorporated into the framework of the GEMTIP model and triaxial ellipsoid inclusions were considered. The depolarization tensors were then examined: **a)** their accuracy was verified, **b)** estimations were enhanced for higher anisotropy, and **c)** the tensors were compared with simplified models. This approach demonstrates significant improvements over simplified unidirectional conductivity models with prolate and oblate ellipsoid inclusions in IP models.

References

Apresyan, L. A. and Vlasov, D. V. (2014). On depolarization factors of anisotropic ellipsoids in an anisotropic medium. *Technical Physics*, 59:1760–1765.

Bérubé, C. L. and Gagnon, J.-L. (2024). Anisotropic induced polarization modeling with neural networks and effective medium theory.

Kittel, C. (2004). *Introduction to Solid State Physics*. Wiley, 8 edition.

Milton, G. W. (2002). *The Theory of Composites*. Cambridge Monographs on Applied and Computational Mathematics. Cambridge University Press, Cambridge.

Pan, E. (2019). Green's functions for geophysics: a review. *Reports on Progress in Physics*, 82(10):106801.

Stroud, D. (1975). Generalized effective-medium approach to the conductivity of an inhomogeneous material. *Phys. Rev. B*, 12:3368–3373.

Zhang, X. and Wu, Y. (2015). Effective medium theory for anisotropic metamaterials. *Scientific Reports*, 5(1):7892.

Zhdanov, M. (2008). Generalized effective-medium theory of induced polarization. *Geophysics*, 73:F197–F211.

Zhdanov, M. S., Burtman, V., Endo, M., and Lin, W. (2018). Complex resistivity of mineral rocks in the context of the generalised effective-medium theory of the induced polarisation effect. *Geophysical Prospecting*, 66:798–817.

jean-luc.gagnon@polymtl.ca